White matter fiber orientation mapping based on T2* anisotropy

J. Lee[1,2], P. van Gelderen[1], L-W. Kuo[1], H. Merkle[1], A. C. Silva[3], and J. H. Duyn[1]
[1]Advanced MRI section/LFMI/NINDS, National Institutes of Health, Bethesda, MD, United States, [2]Department of Radiology, University of Pennsylvania, Philadelphia, PA, United States, [3]CMU/LFMI/NINDS, National Institutes of Health, Bethesda, MD, United States

Introduction

Recent studies have shown that T_2^* relaxation may be anisotropic [1-4]. This anisotropy has been attributed to the microscopic (sub-voxel level) anisotropic distribution of susceptibility perturbers. In white matter fiber bundles, these anisotropic pertubations could originate from compounds such as lipid and ferritin that may align with axons, and could generate magnetic field variations whose magnitude depends on axonal orientation (θ) relative to B_0 [5]. In the current study, we used post-mortem brain tissue to examine the dependence of T_2* on θ and explored the possibility if this dependence could be exploited to map the orientation of white matter fibers analogous to DTI. For these purposes, models were fitted to T_2* measurements at a range of θ values and the fiber orientation map was compared to that derived from DTI.

Background and Method

In gradient echo MRI of brain tissue, transverse relaxation is accelerated by an amount of R_2' ($R_2^* = R_2 + R_2'$) due to local field inhomogeneity caused by microscopic field perturbers. In white matter fiber bundles, the distribution of pertubers may be approached by parallel cylinders causing an angular dependent change of $R_2' = c\Delta\chi\cdot\sin^2\theta$ or $c\Delta\chi\cdot\sin2\theta$. [4-5]. An additional angular dependence may arise from the recently observed "magnetic susceptibility anisotropy" in white matter [7-8]; when susceptibility anisotropy is included, $\Delta\chi$ can be written as $\chi_0 + \chi_a\cdot\sin2\theta$ (planar approximation). Hence, R_2' becomes $[\chi_0 + \chi_a\cdot\sin2\theta]\cdot\sin2\theta$ and R_2^* will show both $\sin2\theta$ and $\sin4\theta$ angular dependency.

Two coronal slabs of a fixed human brain were cut into circular shapes and put in a container. Then cylindrical axis of the container was placed perpendicular to B_0. A 7 T human scanner (GE) with a 3-inch coil was used. The tissues were scanned at 18 different orientations in 10° steps of rotation in the x-z plane. The rotation was performed only in 2D. The sequence was a 3D multi-echo GRE and the scan parameters were TR = 700 ms, TE_1 = 4.6 ms, echo spacing = 2.7 ms (Tissue 1) or 3.0 ms (Tissue 2), # of echoes = 12, FA = 60°, FOV = 8 x 8 x 1.2 cm^3, res = 0.625 x 0.625 x 0.75 mm^3. Each orientation took 23.9 min. For analysis, R_2* values were calculated from multi-echo data and all orientations were realigned to the first image volume using linear and nonlinear registration. Two ROIs were drawn in the corpus callosum area (Fig. 1a) and the average R_2* value was calculated in each ROI in each orientation. The mean R_2* values were fitted with two sinusoidal models: a "$\sin2\theta$ model" with a constant, $\sin2\theta$ and $\cos2\theta$ components and a "$\sin4\theta$ model" with a constant, $\sin2\theta$, $\cos2\theta$, $\sin4\theta$, and $\cos4\theta$ components. Least-square fit results were obtained in each model.

To generate a T_2* fiber orientation map, the model fitted T_2* curve (normalized) was cross correlated on a voxel-by-voxel basis with a 4D T_2* data set (3D space + 18 orientations). The angle of the peak correlation coefficient in each voxel was saved for an angular map. A ΔT_2* map was also generated. Finally, a T_2* orientation map, which color coded the angular map the same as a DTI map and multiplied it by the ΔT_2* map, was generated. For comparison, DTI was acquired at a 7 T animal system with high performance gradient system (450 mT/m in 130 μs). The same resolution and FOV was used and TR = 1000 ms, TE = 57.43 ms, FA = 70°, diffusion gradient direction = 20, b-value of 3,000 s/mm^2. The total scan time was 13.1 hours. The reconstructed DTI results were projected to 2D space to generate a pseudo-2D DTI (a 2D V1 map multiplied by a 2D FA map) and compared to the T_2* orientation map.

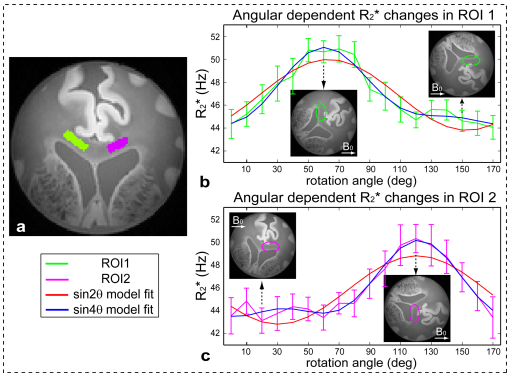

Figure 1. Angular dependent R_2^* in WM

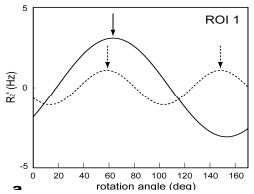

Figure 2. Phase coherence between sin2θ and sin4θ

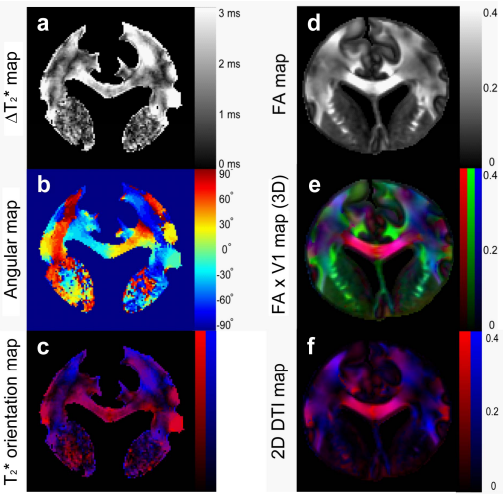

Figure 3. T2* orientation (left) vs DTI (right)

Results

The orientation dependent R_2* variation is shown in Fig. 1. The R_2* curves clearly demonstrate orientation dependency yielding maximum R_2* value when the fibers are oriented perpendicular to B_0. Fitted curves for a $\sin2\theta$ model (red lines) deviate from the measurement (adjusted $R^2 = 0.80 \pm 0.03$) whereas a $\sin4\theta$ model (blue lines) tightly matches to the measurement (adjusted $R^2 = 0.95 \pm 0.01$). The positive peak of $\sin2\theta$ coincides with the positive peak of $\sin4\theta$ (Fig. 2) indicating phase coherence between the two. The ΔT_2*, angular, and T_2* orientation map are shown in Fig. 3 (left column). The ΔT_2^* maps show large ΔT_2* in the areas of large FA values (Fig.3a and 3d). The T_2* orientation map (Fig. 3c) reveals well-known fiber orientation (corpus callosum, STR, and CPT). A great similarity between T_2* orientation results and DTI can also be observed at the bottom rows of Fig. 3 where DTI like color coded T_2* orientation map (Fig. 3c) and pseudo-2D DTI results (Fig. 3f) are shown.

Conclusion and Discussion

In this study, we demonstrated orientation dependent T_2* in ex-vivo white matter and generated a T_2* fiber orientation map. The R_2* curves revealed a $\sin4\theta$ component as well as a $\sin2\theta$ component with phase coherence between the two. A model based on magnetic susceptibility anisotropy yielded a good fit for the measurement. Extension for 3D is straightforward and can be done by rotating tissue in two directions.

Although the $\sin4\theta$ term suggest that susceptibility anisotropy is a significant contributor to R_2', there may be alternative or additional explanations. One possibility is the contribution of "magic angle" effects. When R_2* is modeled by the susceptibility and magic angle effect, the resulting adjusted R^2 was 0.89 ± 0.03. This is lower than that of the anisotropic susceptibility model. Still, it is plausible both susceptibility anisotropy and magic angle effects contribute to the T_2* variation. Interestingly, the anisotropic susceptibility model suggest an unrealistically large anisotropy ($\chi_a/\chi_0 = 0.795$). This may be explained by underestimation of χ_0 either due to deviations from the cylindrical model or cancellation of paramagnetic (e.g. ferritin) and diamagnetic (e.g. myelin lipid) compounds. χ_a may most likely originates solely from myelin (and not ferritin) resulting in an overestimation of χ_a/χ_0.

References [1] Wiggins, ISMRM, 2008, p237 [2] Schafer, ISMRM, 2009, p955 [3], Cherubini, MRM, 2009, p1066 [4] Bender, NMR Biomed, online [5] Yablonskiy, MRM, 1994, p749 [6] Miller, HBM (conference), 2010, Barcelona [7] Lee, PNAS, 2010, p5130 [8] Liu, MRM, 2010, p1471